Fluctuations and Topological Defects in Proper Ferroelectric Crystals

S. Prokhorenko,* Y. Nahas, and L. Bellaiche
Physics Department and Institute for Nanoscience and Engineering, University of Arkansas, Fayetteville, Arkansas 72701, USA
(Received 12 October 2016; published 5 April 2017)

Homotopy theory and first-principles-based effective Hamiltonian simulations are combined to investigate the stability of topological defects in proper ferroelectric crystals. We show that, despite a nearly trivial topology of the order parameter space, these materials can exhibit stable topological point defects in their tetragonal polar phase and stable topological line defects in their orthorhombic polar phase. The stability of such defects originates from a novel mechanism of topological protection related to finite-temperature fluctuations of local dipoles.

DOI: 10.1103/PhysRevLett.118.147601

Topologically nontrivial dipolar configurations are commonly expected to appear in ferroelectric nanostructures (such as dots, films, nanocomposites, rings, or superlattices, see Refs. [1–12] and references therein) as a result of the inherent depolarizing fields arising from surface or interface effects. In the absence of depolarizaing fields, the existence of topological defects can be also expected in structurally disordered materials (e.g., relaxor ferroelectrics [13]) due to strong, randomly distributed, local fields stemming, e.g., from alloying [14]. In both of these cases, topological defects constitute an intrinsic feature of the ground state of the system and correspond to energetically favorable dipolar configurations. On the other hand, topological defects have no reason to appear in systems free of depolarizing and/or local fields, unless granted protection by some alternative, "*topological*", stabilization mechanism. Theoretically, such mechanisms are conventionally related to nontrivial topology of the order parameter (OP) space [15] that can come in play whenever the symmetry of the system is *continuous*. In such cases, continuous symmetry allows the order parameter to swirl and topologically protects intriguing localized patterns like vortices, circulation lines, skyrmions, and monopoles (hedgehogs and antihedgehogs) even at low temperatures where perfect monodomain order is expected [15]. However, ideal ferroelectric crystals exhibit neither local nor depolarizing fields, and the underlying symmetry in these materials is at best *approximately continuous*, especially in *improper* ferroelectric compounds in the vicinity of the critical temperature or in some solid solutions near their morphotropic phase boundary. Therefore, to the best of our knowledge, it is presently unclear if *bulks of proper ferroelectrics* can host stable topological defects in their macroscopic polar phases. If that is the case, it will be also crucial to determine the reason behind the hypothetical existence of stable topological defects in polar phases of proper ferroelectrics.

In this Letter, we use bulk $BaTiO_3$, as a model example, to investigate whether this material can exhibit topological defects. For this, we first resort to the analysis of atomistic effective Hamiltonian simulations via the homotopy theory [16]. Specifically, instead of considering topology of the order parameter (OP) space [15], we investigate the topology of *internal states* manifolds [21] (ISM), which leads us to predict that the nontrivial ISM topology in all ferroelectric phases of $BaTiO_3$ results in the stabilization of topological defects of different dimensionality. Large-scale effective Hamiltonian Monte Carlo simulations are then conducted for bulk $BaTiO_3$ to confirm such novel predictions. Technically, we find that stable defects correspond to pointlike defects with hedgehog or antihedgehog cores in the tetragonal polar phase of $BaTiO_3$ bulk and to linear defects formed by vortex or antivortex cores in its orthorhombic polar phase. The results of our work, hence, reveal a novel mechanism of topological protection, namely the stabilization by finite-temperature fluctuations of local dipoles, that can be realized in proper ferroelectrics. They also provide a theoretical ground for further investigations of topological defects in systems with finite underlying symmetries.

Barium titanate ($BaTiO_3$) bulk is a prototypical proper ferroelectric. Upon cooling, it undergoes a serie of structural phase transitions [22] with a ferroelectric Curie temperature corresponding to the transition from paraelectric ($\mathcal{P}$) to tetragonal ($\mathcal{T}$) phase. The $\mathcal{P}-\mathcal{T}$ transition is then followed by a tetragonal to orthorhombic ($\mathcal{T}-\mathcal{O}$) phase change, with a subsequent symmetry breaking resulting in a rhombohedral ($\mathcal{R}$) ground state. Notably, at each transition, global symmetries of both high- and low-temperature phases are described by two different point symmetry groups, which we will denote by G and H, respectively. In this case, it is easy to see that the corresponding OP spaces, defined as quotient groups G/H [15,23], comprise finite number of elements and are thus endowed with point set topology [16]. For instance, at the $\mathcal{P}-\mathcal{T}$ transition, the order parameter space is topologically equivalent to a set of six *disconnected*

points: G/H comprises six elements related to symmetry-equivalent orientations of a macroscopic polarization in the tetragonal $\mathcal{T}$ phase [[100], [$\bar{1}$00], [010] etc. pseudocubic (p.c.) directions]. Therefore, at each phase transition, the topology of the order parameter space is equivalent to that of a finite set of points. For finite point sets, all the homotopy groups π_n apart from the zeroth homotopy set π_0 [15,23] are trivial and hence, homotopy based classification [15] does not reveal existence of neither point nor linear defects for all ferroelectric phases of $BaTiO_3$ bulk. Moreover, this conclusion should apply not only to $BaTiO_3$ bulks, but also to any proper ferroelectric bulk, at the exception of some solid solutions in their morphotropic phase boundary for which the symmetry might be approximately continuous. For example, it should be valid for *Ti-rich* $Pb(Zr,Ti)O_3$ alloys [24]. On the other hand, recent experiments have revealed that in the Ti-rich $Pb(Zr_{0.2}Ti_{0.8})O_3$ system, local dipoles can nevertheless form continuous vortexlike structures [11] similar to linear topological defects in magnetic systems. The source of this apparent discrepancy may lie in the definition of the OP space that does not allow us to capture continuous rotation of local dipoles away from the symmetry-allowed lattice directions. Therefore, in order to classify topological defects in bulks made of proper ferroelectrics, one may have to explore not the structure of quotient groups G/H, but rather the topology of full internal states manifold [21] that would comprise all values of *local* dipoles accessible within a specific ferroelectric phase.

Here, we explore such possibility and propose to define such internal states manifolds $\mathcal{M}$ via a single variable probability distribution function $\rho(\boldsymbol{u})$ given by

$$\rho(\boldsymbol{u}) = \frac{1}{Z}\int d\hat{\eta}\int d^3\boldsymbol{u}_{i_1}..d^3\boldsymbol{u}_{i_{N-1}}e^{-\beta H_{\text{eff}}(\{\boldsymbol{u}_i\},\hat{\eta})}, \quad (1)$$

where $\boldsymbol{u}_i$ denotes local dipole moments (local modes) in each unit cell $i = 1,\ldots,N$ of a ferroelectric crystal, β corresponds to the inverse temperature in energy units $\beta = 1/kT$, and Z is the thermodynamic partition function. The $H_{\text{eff}}(\{\boldsymbol{u}_i\},\hat{\eta})$ function stands for any effective Hamiltonian describing energy landscape of unstable ferroelectric modes [25,26], and integration in Eq. (1) is carried over all values of strain variables $\hat{\eta}$ (both homogeneous and inhomogeneous), and all except one local mode degrees of freedom. As can be readily seen from its definition, $\rho(\boldsymbol{u})$ gives a probability of any local dipole within a crystal to take a certain value $\boldsymbol{u}$ and can therefore be used to define $\mathcal{M}$ as a set of $\boldsymbol{u}$ values for which $\rho(\boldsymbol{u}) > \varepsilon$, with $\varepsilon \to 0$ being an infinitesimally small positive constant introduced to cutoff internal states with infinitely small occurrence probability. We expect this definition to coincide with the notion of internal states manifold described in Ref. [21], and moreover, to practically allow direct evaluation of $\mathcal{M}$ using standard computational schemes, such as Monte Carlo or molecular dynamics simulations. Here, we resort to Monte Carlo simulations [27] and the first principles based effective Hamiltonian model of Ref. [28] to obtain the topology of the manifolds $\mathcal{M}$ for all distinct structural phases of $BaTiO_3$. The numerical estimate of $\rho(\boldsymbol{u})$ is obtained using $12\times12\times12$ (8640 atoms) periodic supercells and 10^6 Monte Carlo sweeps. The introduction of the finite cutoff ε is necessary in case of numerical evaluation of the integral (1) that is subject to a finite errors in ρ values, as well as artifacts related to finite supercell sizes. However, we expect that sufficiently increasing the supercell size and the accuracy of numerical integration should allow for values of ε at least as low as the numerical precision of computer arithmetic.

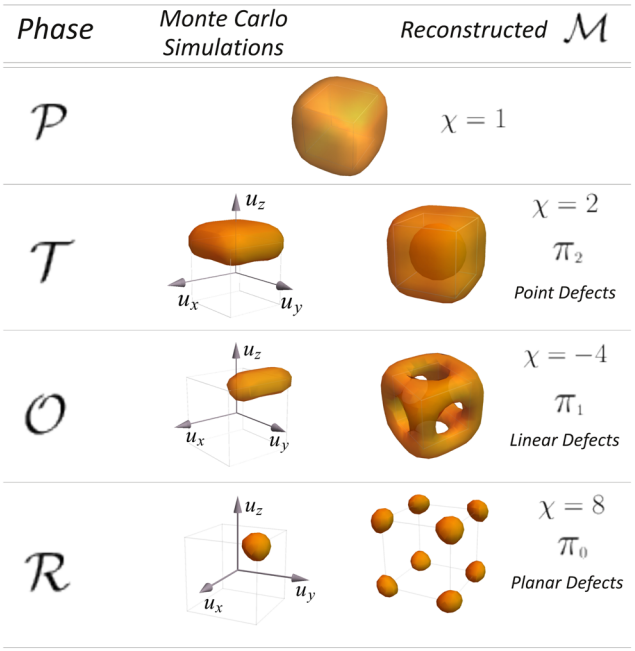

FIG. 1. Regions of finite probability $\rho(\boldsymbol{u}) > \varepsilon$ as obtained from Monte Carlo simulations (second column), and the internal states manifolds $\mathcal{M}$ (third column) for paraelectric ($\mathcal{P}$), tetragonal ($\mathcal{T}$), orthorhombic ($\mathcal{O}$), and rhombohedral ($\mathcal{R}$) phases. The third column also presents the Euler characteristic χ of $\mathcal{M}$, related nontrivial homotopy groups, and the derived stable topological defects. Each symmetry breaking phase transition leads to a rupture of the manifold $\mathcal{M}$, changing its topology as signified by the change of the Euler characteristic χ.

The results of the performed simulations are presented in Fig. 1. It shows three-dimensional plots of $\rho(\boldsymbol{u}) > \varepsilon$ regions obtained from Monte Carlo simulations [with $\varepsilon \sim 10^{-4}$ $(ea_0)^{-3}$, where e and a_0 denote electron charge and Bohr radius, respectively] along with the corresponding reconstructed internal space manifolds $\mathcal{M}$. The necessity of reconstruction of $\mathcal{M}$ from the obtained Monte Carlo data stems from the well-known inability of the Metropolis algorithm to efficiently sample the full configuration space for symmetry-broken phases. Indeed, below transition

temperature, the random walk is usually confined to the configuration space regions corresponding to one single macroscopic order parameter orientation, while the $\mathcal{M}$ set has to include *all* possible local dipole values. Therefore, for $\mathcal{T}$, $\mathcal{O}$, and $\mathcal{R}$ phases, the probability distribution $\rho(\boldsymbol{u})$ obtained from Monte Carlo simulations should be properly symmetrized so as to account for all possible local dipole states. At this point, it is important to note that all the relevant anisotropic energy contributions present in the used H_{eff} model manifest themselves in the symmetry of probability distribution function $\rho(\boldsymbol{u})$ [left column of Fig. (1)] and as a result in the geometry of internal states manifolds [note cuboid shapes in the right column of Fig. (1)]. On the other hand, thermal entropy, being sufficiently high in $\mathcal{T}$ and $\mathcal{O}$ phases, allows local dipoles to significantly deviate from orientations dictated by the anisotropy. As a result, the local symmetry can differ from the macroscopic one, since local dipoles can adopt orientations very different from the direction of global polarization. This possible discrepancy between local and global scales is not taken into account in the traditional picture of topological defects that relies only on the topology of the order parameter space. On the other hand, in the low-temperature $\mathcal{R}$ phase, thermal fluctuations are restricted, and the coinciding local and global symmetries render the internal states and the order parameter manifolds topologically equivalent. To see this, one can reconstruct the order parameter space from the $\rho(\boldsymbol{u})$ function by evaluating polarization $\boldsymbol{P} = \int d^3\boldsymbol{u}\, \boldsymbol{u}\rho(\boldsymbol{u})$ and symmetrizing the resulting single-point set using the cubic point group O_h (paraelectric phase symmetry).

Looking at the results presented in Fig. 1, we see that in the paraelectric phase, $\mathcal{M}$ corresponds to a volume bounded by a cube with rounded edges centered at $\boldsymbol{u} = 0$. The global maxima of ρ are located on the lines corresponding to the rhombohedral polarization directions (i.e., along p.c. $\langle 111\rangle$), while the saddle points are located at orientations corresponding to tetragonal (p.c. $\langle 001\rangle$) and orthorhombic (p.c. $\langle 110\rangle$) polarization orientations. The global minimum is located at the center of coordinate system. Moreover, the set $\mathcal{M}$ is simply connected and homotopy equivalent to a three-dimensional ball. Therefore, the Euler characteristic χ of $\mathcal{M}$ is equal to one, and all homotopy groups π_n of $\mathcal{M}$ are trivial [20].

Interestingly, the symmetry breaking occurring at the $\mathcal{P}-\mathcal{T}$ transition leads to a change of the topology of $\mathcal{M}$. Indeed, below the Curie temperature, the probability of observing local dipoles with small magnitudes vanishes, causing a rupture of $\mathcal{M}$ at $\boldsymbol{u} = 0$ (see third column of Fig. 1). Hence, for the $\mathcal{T}$ phase, $\chi = 2$ and $\mathcal{M}$ are homotopy equivalent to a two-dimensional sphere, meaning that its second homotopy group π_2 is nontrivial ($\pi_2 = \mathbb{Z}$) [20]. At this point, it is worth noting the difference between manifold $\mathcal{M}$ and the corresponding order parameter space. Specifically, the structure of $\mathcal{M}$ (see Fig. 1) suggests that local dipoles significantly deviate from the average polarization value in the tetragonal domains. As a matter of fact, in accordance with the famous Comes-Guinier-Lambert model [29], the probability distribution $\rho(\boldsymbol{u})$ at saddle points located on the Cartesian axes u_x, u_y, and u_z is less than at the maxima corresponding to the $\langle 111\rangle$-equivalent directions. Hence, for the $\mathcal{T}$ phase of $BaTiO_3$, the local dipole moments actually have the freedom to continuously change between domains with different polarization orientation. In contrast, the order parameter space is discrete and describes only the possible *macroscopic* polarization values. This indicates that the suggested insufficiency of the order parameter space to characterize possible complex nanoscale dipolar patterns holds in case of $BaTiO_3$.

The $\mathcal{T}-\mathcal{O}$ transition results in additional ruptures occurring at $\boldsymbol{u}$ corresponding to macroscopic polarization values in the $\mathcal{T}$ phase. The Euler characteristic of the resulting manifold is negative and equals to $\chi = -4$. Moreover, as can be seen from Fig. 1, π_1 is nontrivial in the $\mathcal{O}$ phase; i.e., there are nonequivalent classes of closed loops [15] lying within $\mathcal{M}$. Similarly to the $\mathcal{P}$ and $\mathcal{T}$ phases, ρ has global maxima at the rhombohedral directions and saddle points at orthorhombic directions. Thus, as in the case of the $\mathcal{T}$ phase, the local dipoles within a given orthorhombic domain actually have lower probability to be oriented along the mean polarization direction and effectively fluctuate between several possible rhombohedral ground state orientations. Finally, the phase transition to the $\mathcal{R}$ ground state is marked by ruptures occurring at $\boldsymbol{u}$ equal to polarization values in the $\mathcal{O}$ phase, making the $\mathcal{M}$ manifold a union of eight nonintersecting simply connected volumes. Each of these volumes corresponds to one of the eight equivalent rhombohedral polarization directions, and $\mathcal{M}$ can be practically described by the point set topology. Therefore, for $\mathcal{R}$ phase, the topology of $\mathcal{M}$ is actually equivalent to that of the order parameter space and is therefore characterized by nontrivial zeroth homotopy set π_0 [20,23].

Summarizing the obtained evolution of the internal states manifold $\mathcal{M}$ of $BaTiO_3$ with temperature, we would like to stress several observations. Firstly, at each phase transition, the topology of $\mathcal{M}$ changes, with $\mathcal{M}$ being ruptured at points $\boldsymbol{u}$ corresponding to values of macroscopic polarization in the higher symmetry phase. Secondly, our results show that the $\mathcal{T}$ and $\mathcal{O}$ phases are stabilized by strong thermal fluctuations that enable local dipoles to continuously span a subset of spatial orientations, comprising but not restricted to $\langle 111\rangle$ directions. In this sense, the present analysis goes beyond the Comes-Guiner-Lambert model [29,30]. Finally, the revealed fluctuation statistics show that local dipoles have the freedom to continuously interpolate between symmetry equivalent ferroelectric domains, endowing $\mathcal{M}$ of $\mathcal{T}$ and $\mathcal{O}$ phases with nontrivial topological structure.

The last conclusion requires some additional attention, since it is directly related to stability of topological defects.

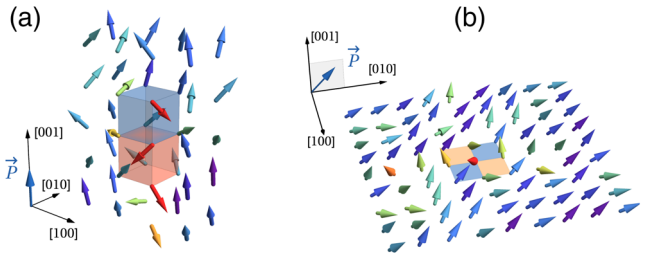

FIG. 2. (a) Dipolar configuration of a hedgehog (antihedgehog) pair in the $\mathcal{T}$ phase at 300 K. Pink and blue unit cells enclose a hedgehog and antihedgehog core, respectively. (b) Configuration exhibiting two vortex (antivortex) pairs in the $\mathcal{O}$ phase at 250 K. Yellow and blue polygons highlight unit cell faces enclosing vortex (antivortex) cores, respectively. In both panels, vector $\vec{P}$ shows the pseudocubic crystallographic orientation of polarization, while colored arrows represent local dipoles ($\boldsymbol{u}$), with blue to red color corresponding to an increasing angle between $\boldsymbol{u}$ and $\vec{P}$.

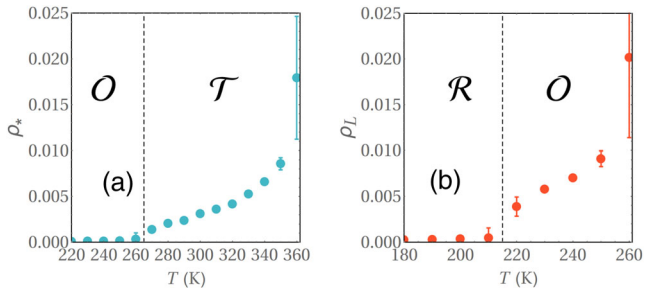

FIG. 3. Calculated temperature dependence of the equilibrium densities of (a) hedgehogs (antihedgehog) pairs in the polar tetragonal phase and (b) vortex (antivortex) pairs in the polar orthorhombic phase. Error bars correspond to standard deviation and whenever are not visible, become smaller than the size of the data points.

Indeed, taking $\mathcal{M}$ in place of order parameter space as codomain in a homotopy-based classification of topological defects [15,23], allows us to reveal that the $\mathcal{T}$ and $\mathcal{O}$ phases can, in fact, exhibit a variety of stable topological defects. Specifically, nontrivial π_2 of $\mathcal{M}$ in the $\mathcal{T}$ phase suggests topological protection of *pointlike* defects [23], such as hedgehog (antihedgehog) cores. On the other hand, in the $\mathcal{O}$ phase, $\mathcal{M}$ is characterized by the nontrivial π_1 yielding protection of *linear* defects [15], e.g., circulation lines composed of two-dimensional vortex or antivortex cores. Finally, in the $\mathcal{R}$ phase, nontriviality of π_0 should yield topological protection of two-dimensional defects, such as domain walls [23], in accordance with discrete topology of the order parameter space. Notably, while the stability of domains walls at low temperatures (in the $\mathcal{R}$ phase of $BaTiO_3$) has been confirmed by first-principles simulations (e.g., see Ref. [31] and references therein), we are not aware of any prediction related to the occurrence of stable point- and linear-defects in its $\mathcal{T}$ and $\mathcal{O}$ phases, respectively.

To check such predictions, we further performed large-scale Monte Carlo simulations using $L \times L \times L$ supercells, with L typically varying between 32 and 58, annealed from $T = 500$ K down to $T = 190$ K with a step of 10 K (using again the effective Hamiltonian of Ref. [28]). At each temperature, the system was relaxed during 10^5 Monte Carlo sweeps, which was sufficient to always obtain a macroscopic polar state. Upon reaching thermal equilibrium, the average densities of hedgehog-antihedgehog pairs ρ_* and vortex-antivortex pairs ρ_L were computed for each considered temperature (at each T, both ρ_* and ρ_L were found to be dynamical, i.e., fluctuating in the course of Monte Carlo sweeps). Examples of such defects obtained from our simulations for $L = 32$, are shown in Fig. 2 (note that similar defects, but of larger size can be also observed once bigger supercell sizes are used as shown in Supplemental Material [16]), while Figs. 3(a) and 3(b) present the calculated temperature dependence of the equilibrium ρ_* and ρ_L for $L = 46$. From Figs. 3(a) and 3(b), one can see that, for 265 K $< T <$ 365 K (corresponding to the stability range of the $\mathcal{T}$ phase within the employed effective Hamiltonian scheme), ρ_* is finite, decreasing as the temperature is reduced within $\mathcal{T}$ until vanishing at, and below, the $\mathcal{T} - \mathcal{O}$ transition (265 K). Moreover, the calculated ρ_L is finite in the $\mathcal{O}$ phase (215 K $< T <$ 265 K), significantly decreasing as the temperature is reduced and eventually vanishing when the $\mathcal{R}$ phase is reached. Therefore, the mere existence of hedgehogs (antihedgehogs) in the $\mathcal{T}$ phase and vortices (antivortices) in the $\mathcal{O}$ phase confirms the prediction of their stability arising from the nontrivial topologies of calculated ISM presented in Fig. 1.

Whereas the new mechanism of topological protection considered in this study is different from the conventional mechanism related to continuous symmetry of the Hamiltonian, the resulting topological defects share many similar features in both cases. Particularly, the conventional decomposition [15] of the energy cost of a defect into the energy of its core (independent of the spatial extent of the defect) and the energy of the deformation of the dipolar field caused by the defect (proportional to the defect size) should hold for $BaTiO_3$ in the same way, it is valid for continuous-symmetry Heisenberg and XY models. Therefore, the physics of topological defects seen in continuous-symmetry models [15] can be also observed in proper ferroelectrics. For instance, in the $\mathcal{T}$ and $\mathcal{O}$ phases, we clearly observe the bonding of hedgehogs (antihedgehogs) and vortices (antivortices), respectively [see Fig. (2) as well as panel (a) of Fig. (1) of Supplemental Material [16]], due to the confinementlike growing of the energy with increasing distance between defects of opposite topological charges.

In summary, in this study, we have explored nontrivial topological defects in ferroelectric phases of $BaTiO_3$ bulks. Our results show that, despite the underlying finite symmetry, the tetragonal and orthorhombic polar phases of this compound can exhibit stable point defects, such as

hedgehog or antihedgehog cores in the $\mathcal{T}$ state and line defects composed of vortex or antivortex cores in the $\mathcal{O}$ phase. Moreover, we have demonstrated that the topological protection of such defects is related to nontrivial topology of the internal states manifolds rather than that of the order parameter space and hence, stems from finite-temperature fluctuations. We thus hope that the present study deepens the current knowledge of the fascinating and active research field devoted to topological defects.

S. P. and L. B. thank the financial support of DARPA Grant No. HR0011-15-2-0038 (under the MATRIX program). Y. N. and L. B. also acknowledge the ARO Grant No. W911NF-16-1-0227.

*prokhorenko.s@gmail.com

[1] A. K. Yadav, C. T. Nelson, S. L. Hsu, Z. Hong, J. D. Clarkson, C. M. Schleputz, A. R. Damodaran, P. Shafer, E. Arenholz, L. R. Dedon, D. Chen, A. Vishwanath, A. M. Minor, L. Q. Chen, J. F. Scott, L. W. Martin, and R. Ramesh, Nature (London) **530**, 198 (2016).
[2] Y. L. Tang, Y. L. Zhu, X. L. Ma, A. Y. Borisevich, A. N. Morozovska, E. A. Eliseev, W. Y. Wang, Y. J. Wang, Y. B. Xu, Z. D. Zhang, and S. J. Pennycook, Science **348**, 547 (2015).
[3] J. J. P. Peters, G. Apachitei, R. Beanland, M. Alexe, and A. M. Sanchez, Nat. Commun. **7**, 13484 (2016).
[4] *Topological Structures in Ferroic Materials: Domain Walls, Vortices and Skyrmions*, edited by J. Seidel (Springer International Publishing Switzerland, Cham, Switzerland, 2016).
[5] Y. Nahas, S. Prokhorenko, and L. Bellaiche,Phys. Rev. Lett. **116**, 117603 (2016).
[6] J. M. Gregg, Ferroelectrics **433**, 74 (2012).
[7] J. F. Scott, A. Schilling, S. E. Rowley, and J. M. Gregg, Sci. Technol. Adv. Mater. **16**, 036001 (2015).
[8] I. Kornev, H. Fu, and L. Bellaiche, Phys. Rev. Lett. **93**, 196104 (2004).
[9] Y. Nahas, S. Prokhorenko, L. Louis, Z. Gui, I. Kornev, and L. Bellaiche, Nat. Commun. **6**, 8542 (2015).
[10] R. K. Vasudevan, Y.-Ch. Chen, Hs.-H. Tai, N. Balke, P. Wu, S. Bhattacharya, L. Q. Chen, Y.-H. Chu, I-N. Lin, S. V. Kalinin, and V. Nagarajan, ACS Nano **5**, 879 (2011).
[11] C.-L. Jia, K. W. Urban, M. Alexe, D. Hesse, and I. Vrejoiu, Science **331**, 1420 (2011).
[12] I. I. Naumov, L. Bellaiche, and H. Fu, Nature (London) **432**, 737 (2004).
[13] Y. Nahas, S. Prokhorenko, I. Kornev, and L. Bellaiche, Phys. Rev. Lett. **116**, 127601 (2016).
[14] S. Prokhorenko, Y. Nahas, and I. Kornev, Phys. Rev. B **90**, 140201(R) (2014).
[15] N. D. Mermin, Rev. Mod. Phys. **51**, 591 (1979); V. P. Mineev, *Topologically Stable Defects and Solitons in Ordered Media* (Harwood Academic Publishing, Amsterdam, 1998); P. M. Chaikin and T. C. Lubensky, *Principles of Condensed Matter Physics* (Cambridge University Press, Cambridge, England, 2000).
[16] See Supplemental Material at http://link.aps.org/supplemental/10.1103/PhysRevLett.118.147601 for a brief overview of homotopy theory, finite size scaling analysis of defect densities and examples of large-scale defects from Monte Carlo simulations, which includes Refs. [17–20].
[17] C. Holm and W. Janke, J. Phys. A: Math. Gen. **27**, 2553 (1994).
[18] E. H. Spanier, *Algebraic Topology* (Springer, New York, 1966).
[19] A. Hatcher, *Algebraic Topology* (Cambridge University Press, Cambridge, England, 2002).
[20] M. Nakahara, *Geometry, Topology and Physics* (Institute of Physics Publishing, London, 2003).
[21] G. Toulouse and M. Kléman, J. Phys. (Paris), Lett. **37**, 149 (1976).
[22] M. E. Lines and A. M. Glass, *Principles and Applications of Ferroelectrics and Related Materials* (Clarendon press, Oxford, 1977).
[23] T. W. B. Kibble in *Proceedings of the NATO Advanced Study Institute on Topological Defects and the Non-Equilibrium Dynamics of Symmetry Breaking Phase Transitions, Les Houches, 1999*, edited by Y. M. Bunkov and H. Godfrin (Springer Netherlands, Dordrecht, Netherlands, 2000), p. 7.
[24] I. A. Kornev, L. Bellaiche, P.-E. Janolin, B. Dkhil, and E. Suard, Phys. Rev. Lett. **97**, 157601 (2006).
[25] K. M. Rabe, C. H. Ahn, and J.-M. Triscone, *Physics of Ferroelectrics: A Modern Perspective* (Springer-Verlag, Berlin, 2007).
[26] K. M. Rabe and U. V. Waghmare, Phys. Rev. B **52**, 13236 (1995).
[27] N. Metropolis, A. W. Rosenbluth, M. N. Rosenbluth, A. H. Teller, and E. Teller, J. Chem. Phys. **21**, 1087 (1953).
[28] L. Walizer, S. Lisenkov, and L. Bellaiche, Phys. Rev. B **73**, 144105 (2006).
[29] R. Comes, M. Lambert, and A. Guinier, Solid State Commun. **6**, 715 (1968).
[30] J. Hlinka, T. Ostapchuk, D. Nuzhnyy, J. Petzelt, P. Kuzel, C. Kadlec, P. Vanek, I. Ponomareva, and L. Bellaiche, Phys. Rev. Lett. **101**, 167402 (2008).
[31] M. Taherinejad, D. Vanderbilt, P. Marton, V. Stepkova, and J. Hlinka, Phys. Rev. B **86**, 155138 (2012).